Current Research in Microbial Sciences 10 (2026) 100600

Contents lists available at ScienceDirect

Current Research in Microbial Sciences

journal homepage: www.sciencedirect.com/journal/current-research-in-microbial-sciences

Probiotic-driven microbiome remodeling is associated with coordinated immune and metabolic responses, improving growth and disease resistance in farmed tongue sole (*Cynoglossus semilaevis*)

Yuanri Hu [a,b,c], Xu Yan [b,c], Fengtao Gao [d], Dan Xu [e], Yingming Yang [a,b,c], Jiayu Cheng [f], Songlin Chen [a,b,c,*], Zhongkai Cui [b,c,*]

[a] College of Fisheries and Life Science, Shanghai Ocean University, Shanghai, 201306, China
[b] State Key Laboratory of Mariculture Biobreeding and Sustainable Goods, Yellow Sea Fisheries Research Institute, Chinese Academy of Fishery Sciences, Qingdao, Shandong 266071, China
[c] Laboratory for Marine Fisheries Science and Food Production Processes, Qingdao Marine Science and Technology Center, Qingdao, 266237, China
[d] Weifang Municipal Key Laboratory of Fishery Resources Development & Comprehensive Utilization, College of Biology and Oceanography, Weifang University, China
[e] School of Ocean, Yantai University, Yantai, 264005, China
[f] Tangshan Weizhuo Aquaculture Co., Ltd., Tangshan, Hebei 063202, China

ARTICLE INFO

Keywords:
Tongue sole
Probiotic
Transcriptomics
Metagenomics
Aquaculture

ABSTRACT

In flatfish aquaculture, labour-intensive tank cleaning represents a major operational challenge, limiting sustainability due to its high labour requirements and associated costs. We tested a new semi-closed recirculating aquaculture system (RAS) protocol for *Cynoglossus semilaevis* (tongue sole), replacing manual cleaning with post-feeding water exchange (80% drained) and probiotic application. Compared with control groups, the probiotic-water exchange protocol significantly improved growth (+0.18%/day) and survival (+7.9%), while shifting the gut microbiota from a *Vibrio*-dominated configuration to a *Photobacterium*-dominated one. Metagenomics revealed that *Photobacterium damselae* became the predominant taxon (86%) in the probiotic group, accompanied by the enrichment of quorum sensing pathways, CAZymes (CEs, AAs), and nutrient metabolism functions. Histological examination showed improvements in the intestinal muscular layer and villi structure. Multi-tissue transcriptomics identified systemic changes in immune and metabolic pathways, including activation of intestinal immune networks (IgA production, NF-κB signaling) and antimicrobial peptide genes. Liver, gill, and skin transcriptomes revealed enhanced DNA repair, cytokine signaling, and barrier pathways. JAK–STAT pathway was also activated, linking microbial metabolite sensing to growth promotion (*stat5b, igf2bp3*). The probiotic-integrated protocol modifies the gut microbiome by shifting microbial composition through changes in competitive interactions and microbial signaling pathways. It also improves the intestinal wall, overall immunity, and nutrient absorption. These findings provide insights into the microbiome-host interaction under probiotic treatment and suggest that this strategy may offer potential benefits under farm conditions, but further studies are needed to validate its safety and ecological implications.

1. Introduction

The sustainable intensification of aquaculture is paramount to meeting global seafood demand (FAO, 2025). Flatfish species such as tongue sole (*C. semilaevis*), prized for its high market value, present significant challenges in traditional farming systems (Wang et al., 2021). A critical bottleneck involves labor-intensive daily maintenance: workers must manually remove accumulated residual feed, feces, and sedimentary debris from concrete tank bottoms (Wang et al., 2009). Failure to perform this meticulous cleaning rapidly degrades water quality, creating an environment conducive to pathogenic outbreaks, particularly vibriosis, often leading to substantial stock mortality (Hu et al., 2020; Li et al., 2019). This relentless requirement for manual intervention translates into prohibitively high operational costs, hindering the economic viability and scalability of *C. semilaevis* production.

To solve this main problem of labor dependence and related risks, we

* Corresponding authors.
E-mail addresses: chensl@ysfri.ac.cn (S. Chen), cuizk@ysfri.ac.cn (Z. Cui).

https://doi.org/10.1016/j.crmicr.2026.100600

Available online 23 April 2026

developed and implemented semi-closed recirculating aquaculture system (RAS) protocol designed for *C. semilaevis*. This protocol combines controlled water exchange and targeted probiotic application. About one hour after feeding, around 80 % of the rearing water is drained, effectively removing most of the suspended organic waste before it settles. A defined multi-strain probiotic consortium is then introduced into the remaining water volume prior to rapid refilling of the system. This method removes the necessity for workers to enter the tanks every day to clean the bottom manually, thereby reducing labour demand and minimizing handling stress.

Probiotics (live microorganisms that confer health benefits to the host) have been used in aquaculture for many years to improve water quality, disease resistance, and growth performance in different species (Lee et al., 2025; Zheng et al., 2025). However, the specific effects of probiotics on host physiological processes remain insufficiently understood (Ding et al., 2022; Mohammed et al., 2025; Nathanailides et al., 2021; Nayak et al., 2020). The precise effects of probiotic administration on key host physiological processes - particularly gut function, systemic immune responses, nutrient metabolism, and growth—remain poorly understood (Bereded et al., 2022; Lee et al., 2023; Naya-Català et al., 2022; Standen et al., 2016). Most studies focus on growth performance or simple changes in the mix of tiny living things inside the body, rather than looking at how the body's own tiny parts change in response to those tiny living things (Guo et al., 2024; Sari et al., 2025; Thy et al., 2017; Xie et al., 2019). Moreover, the interplay between a modified rearing environment (e.g., our water exchange process) and probiotic treatment and its combined effect on the host-microbiome dialogue across multiple organs remains poorly understood.

Thus, in the context of our novel, labor-saving rearing protocol for *C. semilaevis*, this research uses a full multi-omics method to explain the complete effects of probiotic-added water exchange on fish physiology and health. It indicated that this procedure both keeps a great rearing situation and actively changes the host's gut bacteria and body inside, making them grow better and resist sicknesses. To test this, we compared fish raised using the old manual cleaning method with fish raised according to the new probiotic water exchange protocol. We combined: 1) Histomorphological examination of the distal intestine for structural assessment; 2) Gut metagenomic sequencing to give a detailed functional and taxonomic view of the intestinal microbiota, providing insights into microbial composition, metabolic capacity, and pathogen load; and 3) Comparative transcriptomic analysis among key tissues - intestine, liver, gills, and skin - to identify systemic molecular responses. This multi-tissue transcriptomics approach enables us to break down tissue-specific adaptations concerning nutrient metabolism, immune activation (both innate and adaptive pathways), stress response, epithelial barrier function, and detoxification procedures.

This study aims to move beyond descriptive analyses by synthesizing data across different analytical levels to provide an integrated view of how probiotic-associated microbiome remodeling is linked to host physiological responses in *C. semilaevis*. Rather than assuming direct improvements in growth performance and disease resistance, we focus on how the rearing environment influences gut microbiome structure and host physiological responses. This work contributes to a deeper understanding of the intricate host-microbiome-environment interactions in finfish aquaculture. Importantly, this protocol has already been implemented in commercial-scale farming systems, offering an opportunity to evaluate microbiome-host interactions in realistic aquaculture conditions. However, further studies are needed to confirm its practical benefits, safety, and ecological implications.

2. Method and materials

2.1. Ehics statement

This research adhered to the principles outlined in the Experimental Animal Care, Ethics and Safety Inspection Protocol of the Yellow Sea Fisheries Research Institute, Chinese Academy of Fisheries Sciences (Authorization Code: YSFRI-2025,017). All experimental procedures were carried out in compliance with applicable guidelines and standards, and follow the ARRIVE guidelines. For humane euthanasia, tongue sole designated for sampling or reaching the experimental endpoint were anesthetized with an overdose of MS-222 and kept immersed for a minimum of 10 min following the cessation of gill movement.

2.2. Tongue sole and trial design

Tongue sole individuals (~200 g, ~30 cm) were sourced from Hebei Weizhuo Aquaculture Co., Ltd. A total of 6000 fish were randomly allocated into control (CG) and experimental (EG) groups, with three replicates per group (1000 fish per replicate). The experiment was conducted in six aquaculture tanks (5 × 7 × 1 m) maintained at a water depth of 40 cm. Water quality parameters were monitored throughout the experimental period to ensure environmental stability. Water temperature was maintained at 21 ± 2 °C and continuously monitored using a high-precision digital thermometer (Hengshui Zhengxu Electronic Technology Co., Ltd., China). Salinity was maintained at 20 ± 2.8 ‰ and measured once daily. Dissolved oxygen was maintained above 10 mg/L through continuous aeration using a blower system. Water pH was maintained between 7.0 and 8.0 and measured daily using pH test strips (Hangzhou Shisan Technology Co., Ltd., China). Ammonia nitrogen concentrations ranged from 0.09 to 0.15 mg/L and were measured every four days using a commercial test kit (Yancheng Bainuo Biotechnology Co., Ltd., China). Nitrate concentrations ranged from 0.04 to 0.45 mg/L and were also measured every four days using the same type of test kit. The experimental design was implemented: Control group without probiotic supplementation; Experimental group supplemented with commercial probiotic compound (*Bacillus subtilis*, and *Rhodopseudomonas palustris*). Two commercial probiotic products, Yuminle Guangsubao and Yuminle Aquatic Bacillus 1000 (Guangdong Wanghai Biotechnology Group, China), were used in combination for water treatment. Prior to application, the probiotics were activated according to the manufacturer's instructions. The activated products were then added directly to the rearing water on a daily basis. Under the experimental conditions (approximately 14 m^3 of water volume per tank), the final concentrations were approximately 3×10^6 CFU/L for *Bacillus* spp. and 3×10^5 CFU/L for *R. palustris*. The probiotic mixture was applied uniformly to ensure even distribution throughout the water column. Fish were fed twice daily (6:00 and 18:00). One hour post-feeding, tank water was drained to 8 cm depth, followed by application of 500 L of compound photosynthetic bacteria or plain water (Fig. 2A). The water inlet valve was then reopened. The trial lasted three months. At harvest, individual body weights of surviving fish were recorded. Six tanks were used in total, with three independent tank replicates per treatment (control and experimental groups). For growth performance analysis, 30 fish were randomly sampled from each tank at the end of the experiment to measure body weight. The mean value per tank was calculated and used as the statistical unit ($n = 3$ tanks per group), thereby avoiding pseudo-replication. Specific growth rate (SGR) was calculated as:

$$SGR = \left(e^{\frac{\log_e(w2) - \log_e(w1)}{T}} - 1 \right) \times 100$$

where W1 and W2 are initial and final weights, and T is the trial duration (Grane et al., 2020). In addition, other growth performance parameters were calculated as follows:

Weight gain rate (WGR, %) = $100 \times (W_2 - W_1) / W_1$

2.3. Sample collection

For metagenomic investigation, 50 mg of gut content were sampled from the same region of the distal gut from 18 individuals, including 9

samples from control group and 9 samples from experimental group. Samples were immediately frozen on dry ice and subsequently transferred to $a-80$ °C freezer within hours. For transcriptome analysis, 50 mg of skin, intestine, liver and gill were sampled from 18 individuals, including 9 samples from control group and 9 sample from experimental group. All samples were immediately frozen in liquid nitrogen. For histological profiling, histological sections of control and experimental fish were performed. 100 mg of gut was dissected and fixed in paraformaldehyde at 4 °C. For sectioning, tissues were dehydrated and embedded in paraffin. Samples were serially sectioned at 6∼8 um thickness and stained using hematoxylin-eosin (HE). Following the method described by Qu (Qu et al., 2025), ImageJ software (Version 1.53) was employed for the quantitative assessment of villus thickness and muscularis thickness. Briefly, for each intestinal histological section, measurements were taken from at least five fields of view at the narrowest region of the villi and the thinnest region of the muscularis layer, and the mean values were calculated to represent the section. These measurement data were analyzed using descriptive statistics and the Mann-Whitney U test due to non-normal distribution in both groups (Shapiro-Wilk test, $p < 0.05$). Variance homogeneity was confirmed (Levene's test, $p > 0.05$).

2.4. Metagenomic data generation

Prior to analysis, all samples were randomized. Microbial genomic DNA was extracted from a total of 18 tongue sole gut content samples (9 control and 9 experimental). Genomic DNA was extracted from intestinal content samples using the HiPure Stool DNA Kit (Magen, China) according to the manufacturer's instructions. Briefly, approximately 150–200 mg of intestinal content was subjected to mechanical and chemical lysis, followed by protein digestion and column-based DNA purification. DNA was eluted in sterile buffer and stored at −20 °C until further processing. DNA quality and integrity were assessed using a NanoDrop 2000 spectrophotometer (Thermo Fisher Scientific, USA) and agarose gel electrophoresis. Samples with A260/A280 ratios between 1.8 and 2.0 and A260/A230 ratios above 1.8 were considered acceptable for downstream analysis. Metagenomic libraries were constructed using the NEBNext® Ultra™ DNA Library Prep Kit for Illumina (New England Biolabs, USA). Briefly, genomic DNA was fragmented to an appropriate size, followed by end repair, phosphorylation, and A-tailing. Sequencing adapters were ligated to the DNA fragments, and fragments of approximately 300–400 bp were selected using AMPure XP beads (Beckman Coulter, USA). Libraries were then enriched by PCR amplification under the following conditions: initial denaturation at 98 °C for 30 s, followed by 12 cycles of 98 °C for 10 s, 65 °C for 75 s, and 72 °C for 30 s, with a final extension at 72 °C for 5 min. Library quality was evaluated using an Agilent 2100 Bioanalyzer (Agilent Technologies, USA), and libraries showing a single peak of expected size distribution were selected. Library quantification was performed using a real-time PCR system (ABI StepOnePlus, Life Technologies, USA). Sequencing was performed on the Illumina NovaSeq X Plus platform using a paired-end 150 bp (PE150) strategy.

2.5. Metagenomic bioinformatics: filtering, assembly, binning, refinement, and functional analysis

A subset of the data generated for this study was utilized in a separate, comparative investigation. The data processing methodology was detailed in Rasmussen et al. 2021 (Rasmussen et al., 2021). Raw sequence reads underwent quality control using FASTP (version 0.18.0) (Chen et al., 2018) to assess filtering steps and read quality. Adapter removal and elimination of low-quality reads were performed using AdapterRemoval v2.2.4 (Schubert et al., 2016), with a base quality threshold of 30 and a minimum read length of 50 bp. Duplicate reads were removed, and reads were re-paired to exclude singletons using BBMap v38.35 (Bushnell., 2014). To enhance assembly efficiency by reducing eukaryotic contaminants, the data were filtered against the PhiX174 genome, the human genome (HG19), and the tongue sole genome using Minimap2 (Li et al., 2016). Filtered reads were then subjected to both single assembly and co-assembly using MEGAHIT v1.1.1 (Li et al., 2015). Assemblies were performed with the meta-sensitive flag for metagenomic purposes, setting a minimum scaffold length of 1000 bp. The quality of the assembled contigs was assessed using QUAST v5.02 (Mikheenko et al., 2016). To improve binning efficiency, we employed the anvi'o pipeline (Eren et al., 2015). The relative abundance of each Metagenome-Assembled Genome (MAG) was calculated based on the percentage of reads recruited across all samples from the specific host. Within anvi'o, scaffolds were profiled using Prodigal v2.6.3 (Hyatt et al., 2010) with default parameters to identify genes. These genes were then matched against archaeal (Lee et al., 2019), protistan (based on http://merenlab.org/delmont-euk-scgs), and bacterial (Lee et al., 2019) single-copy core gene collections using HMMER v3.3.2. Additionally, ribosomal RNA genes were identified using HMMs sourced from Barrnap (https://github.com/tseemann/barrnap). MAG completeness and redundancy (contamination) were estimated based on the presence of single-copy core genes (SCGs) within the anvi'o databases. Predicted gene functions were annotated using Pfam (El-Gebali et al., 2019), COG (Tatusov et al., 2000) and KEGG (Kanehisa et al., 2016) databases. Analyses of COG coverage across the whole metagenome were conducted using Tukey's Honestly Significant Difference (HSD) test. The composition of COGs across different feeding types and samples was visualized using a network-based approach implemented in Gephi v0.9.2 (Bastian et al., 2009). Functional networks were generated by connecting COG functions to samples using the Force Atlas 2 algorithm, running for 20,000 iterations. Differential abundance analysis of all genes recovered from MAGs was performed using generalized linear models (GLMs) in DESeq2 (Love et al., 2014) within the R environment. To account for multiple testing, p-values were adjusted using the Benjamini-Hochberg false discovery rate (FDR) correction (Benjamini et al., 1995).

2.6. Detection of photobacterium damselae using multiplex PCR

Based on the metagenomic sequencing result, we would like to confirm whether *P. damselae* exists in the intestines of the tongue sole and which subspecies it belongs to. Samples included 3 backup intestinal content samples from the experimental group and 21 freshly collected intestinal contents, consisting of 15 samples obtained from 5 different aquaculture company employing a probiotic rearing regime and 6 samples obtained from 2 aquaculture company employing a non-probiotic rearing regime. Total genomic DNA was extracted from the freshly collected intestinal contents using the TIANamp Stool DNA Kit (Tiangen Biotech (Beijing) Co., Ltd., China) in accordance with the manufacturer's instructions. According to previous report (Shao et al., 2019), *P. damselae* can be identified and the two subspecies, *P. damselae* subsp. *damselae* and *P. damselae* subsp. *piscicida*, can be differentiated based on the *ureC* and *Car* genes (*P. damselae* subsp. *damselae* yields PCR amplicons for both the *ureC* (448 bp) and *Car* genes (267 bp), whereas *P. damselae* subsp. *piscicida* produces an amplicon only for the *Car* gene). Therefore, multiplex PCR was performed using primers targeting both the ureC and Car genes. Each 50 μL amplification reaction consisted of 1.5 μL of each primer (Ure-F, Ure-R, Car-F, and Car-R), 17 μL ultrapure water, 25 μL PrimeSTAR Max DNA Polymerase (TaKaRa), and 2 μL template DNA. The thermal cycling program included an initial denaturation at 95 °C for 3 min, followed by 30 cycles of 98 °C for 10 s, 52.5 °C for 15 s, and 72 °C for 10 s, with a final extension at 72 °C for 5 min. The PCR primer sequence are listed in Table 1.

2.7. Transcriptome analysis

We sequenced and analyzed the transcriptome using methods consistent with our previous studies (Hu et al., 2022). Briefly, total RNA

Table 1
Multiplex PCR Primers used in this study.

Primer	Sequence (5′-3′)	Reference
ureC-F	TCCGGAATAGGTAAAGCGGG	Shao et al., 2019
ureC-R	CTTGAATATCCATCTCATCTGC	
Car -F	GCTTGAAGAGATTCGAGT	Shao et al., 2019
Car-R	CACCTCGCGGTCTTGCTG	

was extracted from skin, intestine, liver, gill, and kidney tissues using TRIzol reagent following the manufacturer's instructions. RNA quality and integrity were assessed using agarose gel electrophoresis and an Agilent 2100 Bioanalyzer, and samples with RNA integrity number (RIN) > 7.0 were used for library construction. Sequencing libraries were prepared using the Illumina TruSeq RNA Sample Preparation Kit and sequenced on an Illumina platform to generate paired-end reads. Raw reads were processed to remove adapters and low-quality sequences using Trimmomatic (v0.39). Clean reads were then mapped to the reference genome of *C. semilaevis* (NCBI Taxonomy ID: 244,447) using HISAT2 (v2.2.1). Gene expression levels were quantified as fragments per kilobase of transcript per million mapped reads (FPKM) using StringTie (v2.1.4). Differential expression analysis was performed using DESeq2 (v1.30.1), with genes considered differentially expressed at $|\log2$ fold change$| > 1$ and p-value < 0.05. Functional enrichment analysis of differentially expressed genes (DEGs) was conducted using KEGG pathway analysis, with significance determined at $p < 0.05$.

2.8. Challenge test

To validate the role of candidate genes from our transcriptome analysis in pathogen response, we selected a subset, formulated their mRNAs into lipid nanoparticles (LNPs), and intraperitoneally injected them into fish. The preparation method of LNP is as described by Wang (Wang et al., 2023). The LNPs components were dissolved in 100 % ethanol with the following molar ratios: 50 mol % 1-octylnonyl 8-[(2-hydroxyethyl)[6-oxo-6-(undecyloxy)hexyl]amino]-octanoat (SM102), 10 mol % 1,2-Distearoyl-sn-glycero-3-phosphocholine (DSPC), 38.5 mol % cholesterol (CHO) and 1.5 mol % 1,2-dimyristoyl-rac-glycer-o-3-methoxypolyethylene glycol-2000(DMG-PEG2000). The mRNA synthesis is provided by GenScript and the mRNA dissolved in 50 mM acetate buffer (pH=4.5). The mRNA solution (Detailed information on the sequence can be found in Supplementary Materials) was added into the lipid using the vortex mixing method (total lipids/mRNA = 40/1, wt/wt; total lipids/mRNA=1/3, V/V). And then this formulation was further dialyzed against PBS (10 mM, pH 7.4) overnight at 4 °C. After 24 h of injecting LNPs, these fish were subjected to an intraperitoneal injection with 150 μL of a live *V. harveyi* suspension (1.0×10^9 cells/mL). The bacterial strain, originally isolated from diseased fish and maintained in our laboratory, was cultured in tryptic soy broth (TSB) at 28 °C until reaching the mid-logarithmic phase. The bacteria were then harvested via centrifugation and resuspended in phosphate-buffered saline (PBS) for the challenge. For the challenge experiment, healthy fish from the control population were randomly assigned to three treatment groups: PBS + challenge, empty LNP + challenge, and LNP-ccl19 + challenge. Each treatment included three independent replicates, with 50 fish per replicate. Fish in the experimental group were intraperitoneally injected with ccl19 mRNA encapsulated in LNPs, while control fish received either PBS or empty LNPs. Mortality was recorded daily for 7 days. Survival curves were generated using the Kaplan–Meier method, and differences among groups were analyzed using the log-rank test. A p-value < 0.05 was considered statistically significant. Kaplan-Meier curves were generated using the *survminer* package in R (v4.3.3).

2.9. Integration analysis

To explore the associations among gut microbiota parameters, intestinal differentially expressed genes (DEGs), and host phenotypic traits — specifically body weight and survival rate across experimental groups — an integrated correlation analysis was performed.

Initially, bivariate Pearson correlation analysis was conducted to evaluate relationships between host phenotypic traits (body weight and survival rate), gut microbiota parameters (focusing on the top 80 most abundant microbial taxa), and host variables, including DEGs. This analysis was carried out using SPSS Statistics version 24.0. Statistically significant correlations ($p < 0.05$) were subsequently visualized as clustered heatmaps via the OmicShare online platform (https://www.omicshare.com/).

Subsequently, network-based analyses were employed to elucidate complex interactions. Specifically, a KEGG pathway-DEG interaction network was constructed using the integrated Cytoscape module within the OmicShare platform. Concurrently, a microbial co-occurrence network was generated using the CNSknowall platform (https://cnsknowall.com/), based on SparCC correlation analysis with stringent thresholds ($|r| > 0.8$, $p < 0.01$).

2.10. Real-time qPCR validation

To ensure the reliability of the transcriptome sequencing data, the expression patterns of six genes from intestine were validated using the SYBR® Premix Ex Taq™ (TaKaRa, Japan) on an ABI 7500 Fast Real-Time PCR system (Applied Biosystems, USA). The thermal cycling conditions were as follows: 95 °C for 30 s, followed by 40 cycles of 95 °C for 15 s, 60 °C for 20 s, and 72 °C for 10 s. β-actin and gadph were served as the internal control for normalization (Cui et al., 2017; Ma et al., 2015). Relative expression was calculated using the Pfaffl method with normalization to two reference genes, following the procedure described on toptipbio.com (https://toptipbio.com/qpcr-multiple-reference-genes/). Amplification efficiency (E) values were obtained from standard curves. For each sample, ΔCt was calculated as Calibrator Ct − Sample Ct, and relative quantity (RQ) was computed as $RQ = E^{\Delta Ct}$. A normalization factor was determined as the geometric mean of the RQ values of the two reference genes. The relative expression level of the target gene was then calculated as RQ_{target} /geometric mean of reference RQs, with the control group set to 1.0. Each sample was analyzed in triplicate, and statistical significance was assessed using Prism software, which was also used to generate the plots. The specific primer sequences, primer's R^2 and the primer amplification efficiency are listed in Table 2.

2.11. Statistical analysis

All statistics were conducted using R (version 3.6.1) and Python (version 3.7.4). For growth performance and survival rate, tank means were used as biological replicates ($n = 3$ per group). Differences between

Table 2
RT-PCR Primers used in this study.

Primer	Sequence (5′-3′)	R^2	E/ %
stat5b-RT-F	GAGTCTGTGACGGAGGAG	0.991	92
stat5b-RT-R	TGGCTGTGGCATTGTTAT		
igf2bp3-RT-F	AGTGGGAGGTTTTGGACA	0.993	108
igf2bp3-RT-R	TCGGACATTGACGACTGC		
acot2- RT-F	TGAGATTCACCTGGATTA	0.997	105
acot2-RT-R	ACCCGACTCTTTTACTGC		
ccl19- RT-F	AGACACTCTGAGGAGCATCG	0.992	107
ccl19-RT-R	CAGGTGGACTGAGGGTTC		
mrc1-RT-F	TGTGCAGTGATGATGGAA	0.990	99
mrc1-RT-R	CCGTTGCTGGCAGTGTAA		
IL1R2-RT-F	GAATGCGAAATGGCCGACTC	0.992	108
IL1R2-RT-R	CTCGCTCATCCAGGTACGAC		
β-actin-RT-F	TTCCAGCCTTCCTTCCTT	0.998	90
β-actin-RT-R	TACCTCCAGACAGCACAG		
gadph-RT-F	ACGGTGATTGCCACTCCTCC	0.992	90
gadph-RT-R	GTCGCAGACACGGTTGCTGT		

groups were evaluated using two-tailed Student's *t*-tests. Data are presented as mean ± standard deviation (SD), and differences were considered statistically significant at $p < 0.05$.

3. Results

3.1. Probiotic treatment enhances growth performance and survival rate

The tongue sole were administered compound probiotics for three months. Post-treatment measurements revealed a 0.18 %/day (Fig.1C, $p < 0.05$) increase in growth rate compared to the control group (Weight gain rate: 80.96 ± 3.9 % vs 59.85 ± 3.82 %, Fig. 1B, $p < 0.05$), with average weights of 283.7 ± 15.4 g (experimental group) and271.5 ± 18.1 *g* (control group). Additionally, feed intake was higher in the probiotic-treated group (514.6 ± 52.8 g vs. 434.69 ± 35.3 g, (Fig.1A), $p < 0.05$). The survival rate of the experimental group was (97.17 ± 0.87) %, while that of the control group was (89.27 ± 0.95) % (Fig.1D, $p < 0.05$).

3.2. Probiotics improve intestinal condition

Following the supplementation of probiotics in the water, the intestinal muscularis thickness of the experiment group of C. *semilaevis* showed a significant increasing trend (124.57± 37.97 vs. 108.39 ± 20.89 μm, $p < 0.05$). Histological sections of the intestine revealed that, compared to the control group, the muscularis layer in the experiment group was notably thicker (387.35± 101.59 vs. 314.27 ± 94.75 μm, $p < 0.05$) (see Fig. 2B-F). Furthermore, detailed observations indicated a widening of the folds in some intestinal goblet cells in the probiotic-treated group.

3.3. Probiotic application alters gut microbial compositions

During the experiment, the tongue sole received probiotic baths after feeding, whereas the control group did not. Comparative analysis revealed a significant shift in gut microbiota composition between groups: the control group was dominated by *Vibrio*, whereas the experimental group exhibited a higher relative abundance of *Photobacterium*. Over 94 % of the identified species were bacterial, with *Photobacterium* comprising ~86 % of the microbiota in the probiotic-treated group, compared to ~88 % *Vibrio* in the control group (Fig. 3A, This result was obtained by excluding the bacteria that could not be classified in the calculation.). To confirm whether *P. damselae* exists in the intestines of the tongue sole and which subspecies it belongs to, among all samples (three backup intestinal content samples from the experimental group and the twenty-one freshly collected intestinal content samples) collected to date, only the *Car* gene amplicon (267 bp) was successfully amplified (Fig. 4E), whereas no amplification product was obtained for the *ureC* gene. These results confirm that the *P. damselae* strains detected in the intestinal samples of tongue sole belong to *P. damselae* subsp. *Piscicida* (The electrophoresis results serve only a qualitative purpose), with no evidence of the presence of *P. damselae* subsp. *damselae*.

Principal coordinates analysis (PCoA) demonstrated distinct clustering of microbial communities, with 99.99 % of variance explained by two principal components (Fig. 3B). Alpha-diversity analysis (Chao1, ACE, Simpson, and Shannon indices) indicated significantly higher microbial diversity in the control group (Fig. 3C-F). LEfSe analysis further

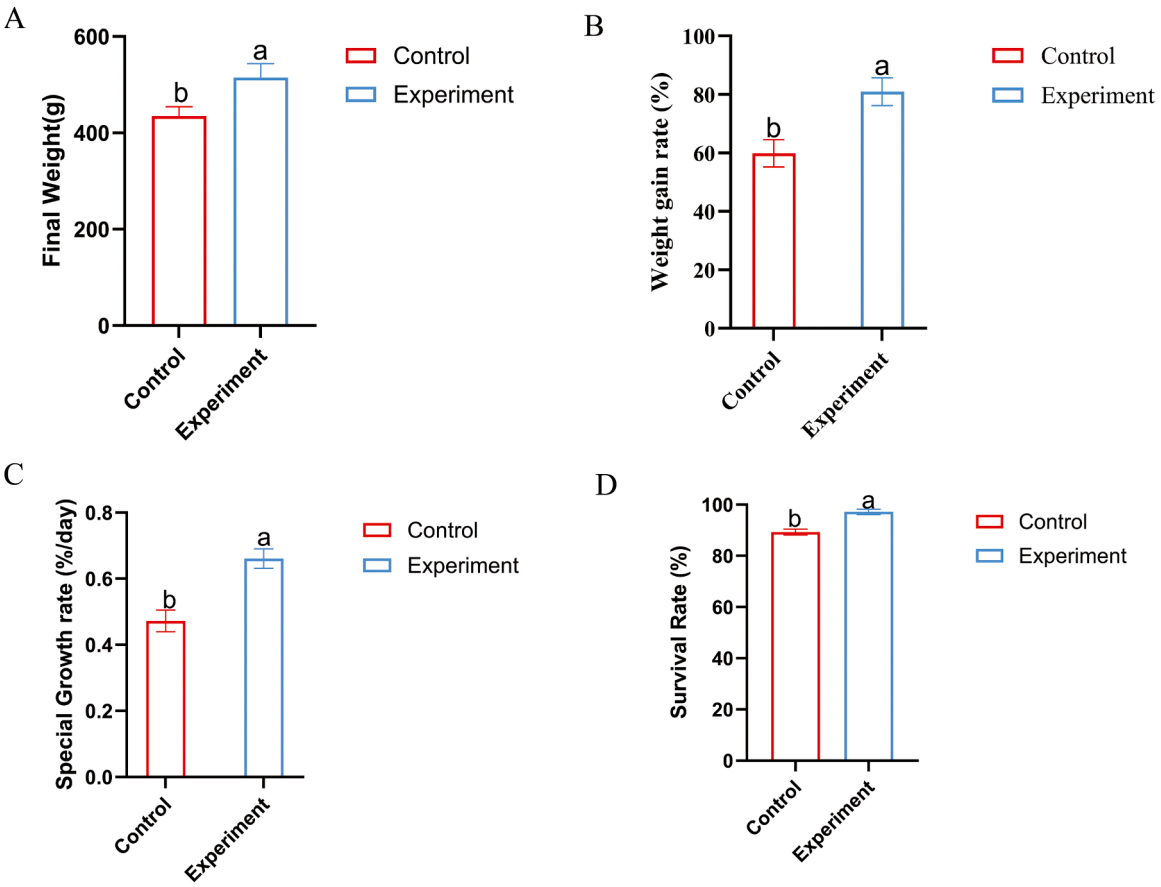

Fig. 1. Growth performance and survival rate of Cynoglossus semilaevis under probiotic treatment. (A) Final body weight (g) of the control and experimental groups. (B) Weight gain rate (%) in the control and experimental groups. (C) Specific growth rate (%/day) for the control and experimental groups. (D) Survival rate (%) in the control and experimental groups. Data are presented as mean ± SD. Different letters (a, b) above bars indicate significant differences between groups ($p < 0.05$).

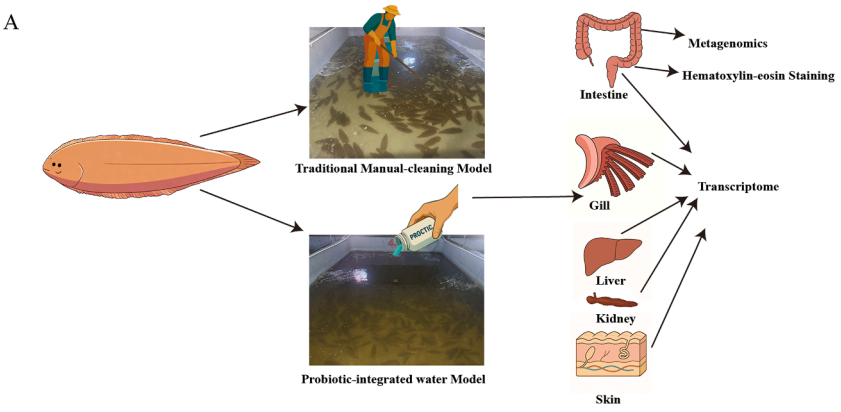

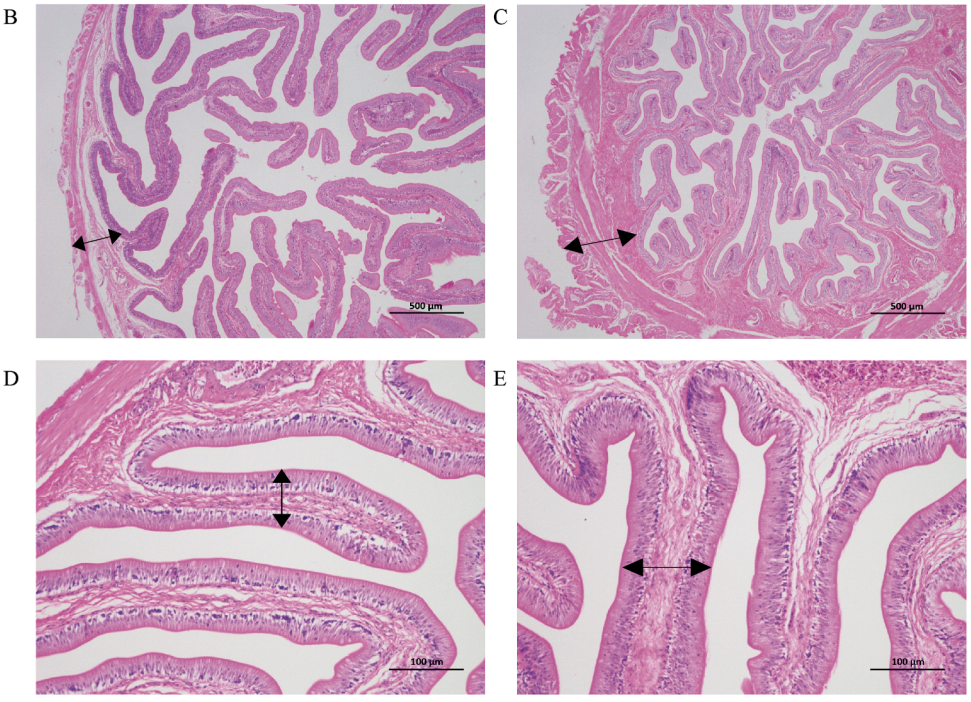

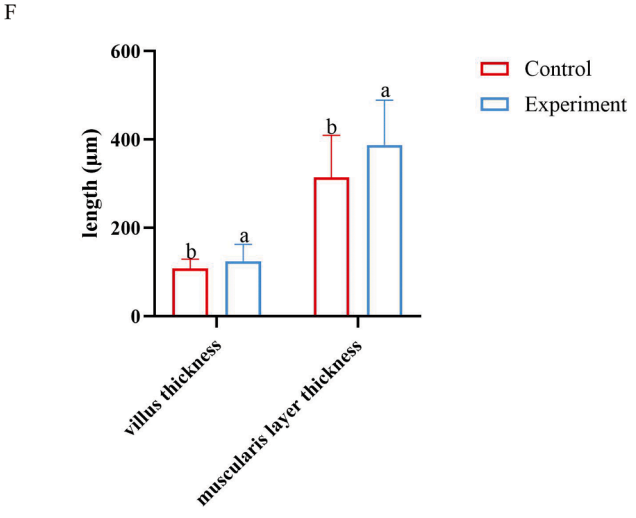

(caption on next page)

Fig. 2. Comparison of traditional manual-cleaning model and probiotic-integrated water model in aquaculture. (A) Schematic illustrating the two aquaculture models: traditional manual-cleaning model (top) versus probiotic-integrated water model (bottom). The arrows indicate the flow of experimental methods: metagenomics (intestine), hematoxylin-eosin staining (intestinal tissue), and transcriptomics (gill, liver, kidney, skin). Key differences between the two models are highlighted, with probiotics being applied in the experimental group. Histological analysis of intestinal tissues in *C. semilaevis.* Hematoxylin–eosin (H&E) staining of distal intestine sections from the control group (CG) and experimental group (EG). (B–C) Low-magnification images (scale bar = 500 μm) showing overall intestinal morphology. Arrows indicate the muscularis layer. (D–E) High-magnification images (scale bar = 100 μm) highlighting epithelial integrity and villus structure. Arrows indicate villus thickness. Representative images from each group are shown. (F) Villus thickness and muscle thickness measurements between control group and experiment group. Data are presented as mean ± SD. Different letters (a, b) above bars indicate significant differences between groups ($p < 0.05$).

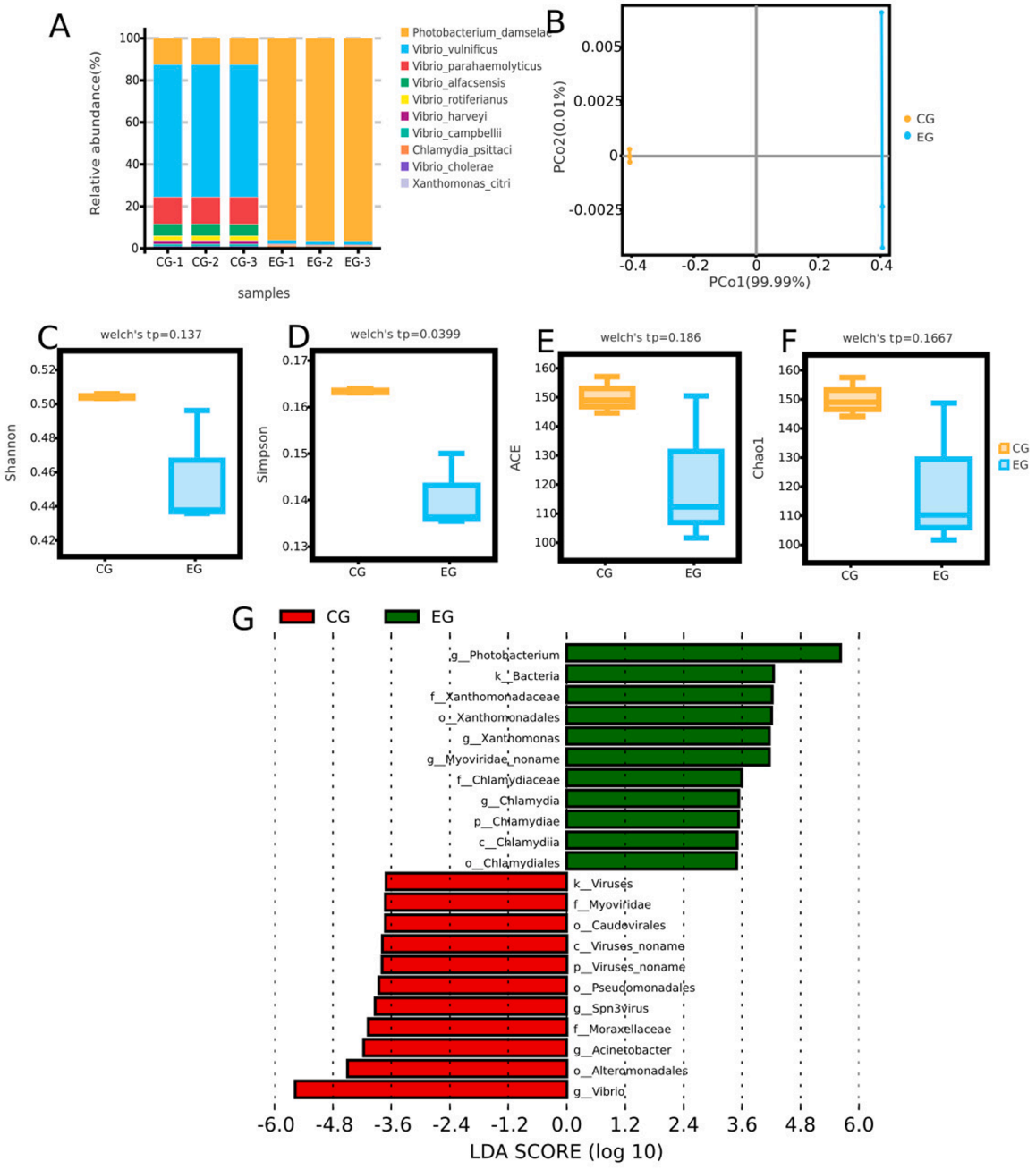

Fig. 3. Analysis of the composition of the gut metagenomic microbiota. (A) Microbiome composition at the species level samples in control (CG) and experimental (EG) groups. (B) Principal coordinates analysis (PCoA) based on Bray–Curtis distance, showing separation of microbial communities between groups. (C–F) Alpha diversity indices, including Shannon, Simpson, ACE, and Chao1. (G) Linear discriminant analysis effect size (LEfSe) identifying differentially enriched taxa between groups.

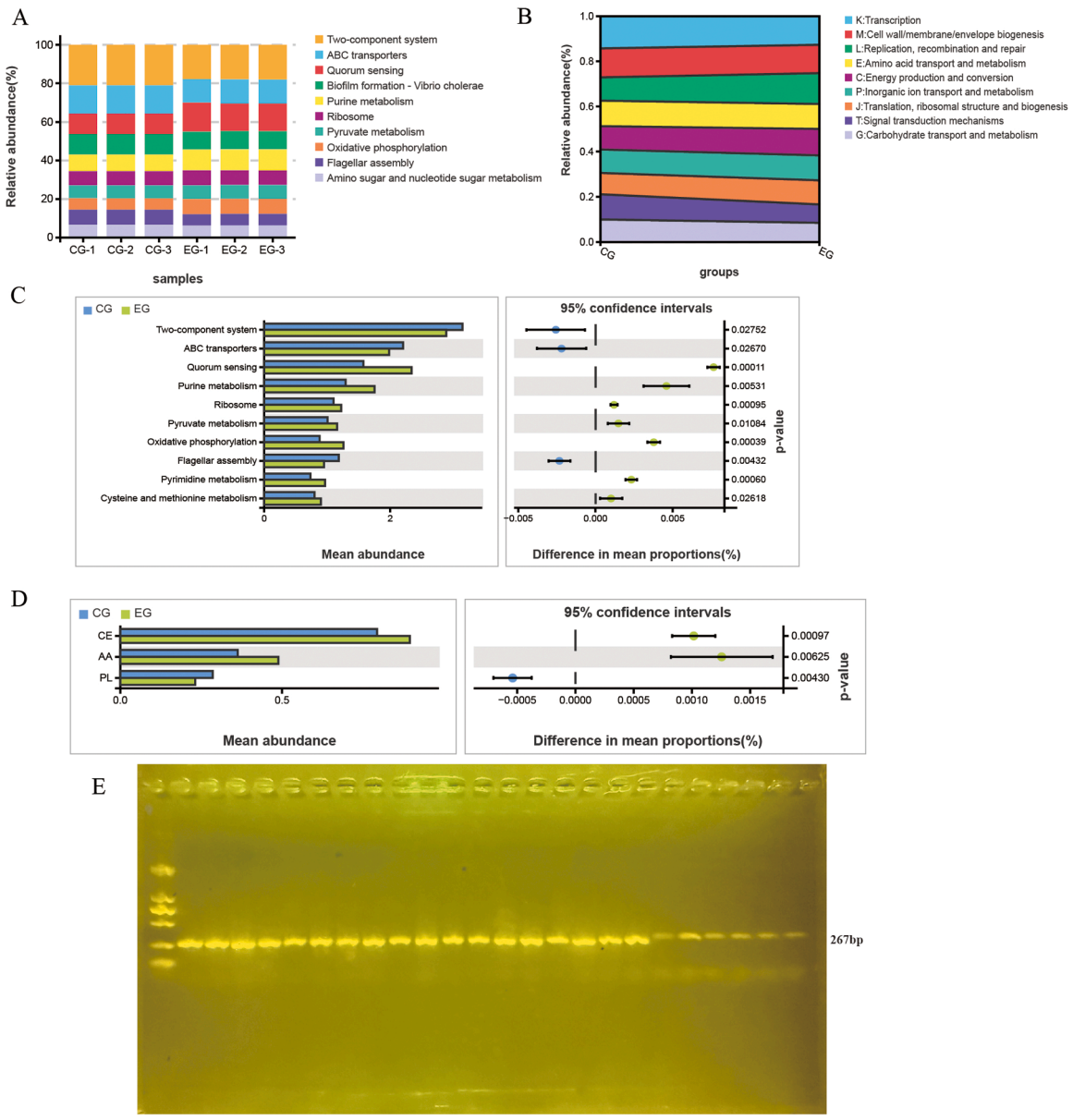

Fig. 4. Functional profiling of gut metagenomic microbiota. (A) Relative abundance of the top 10 KEGG pathways in control (CG) and experimental (EG) groups. (B) Functional classification based on eggNOG annotation. (C) Differential analysis of KEGG pathways between groups. (D) Differential analysis of carbohydrate-active enzymes (CAZy), including CE and AA classes. Statistical significance was assessed using appropriate statistical tests ($*p < 0.05$). (E) Multiplex PCR amplification in 3 backup intestinal content samples from the experimental group and 21 freshly collected intestinal contents, consisting of 15 samples obtained from 5 different aquaculture company employing the probiotic breeding model and 6 samples obtained from 2 aquaculture company employing traditional breeding model.

confirmed *Photobacterium* as a key biomarker in the experimental group, while *Vibrio* predominated in controls (Fig. 3G).

3.4. Probiotics modulate metabolic and functional pathways

Metagenomic sequencing of digestive tract contents revealed significant differences in KEGG-enriched pathways, including two-component systems, ABC transporters, quorum sensing, *Vibrio cholerae* biofilm formation, and purine metabolism (Fig. 4A and Fig. 4C). eggNOG analysis indicated enhanced activity in replication, recombination, and repair processes in the probiotic-treated group (Fig. 4B).

Furthermore, CAZy analysis demonstrated elevated enzymatic activity (CE and AA classes) in the experimental group, suggesting improved nutrient metabolism (Fig. 4D). This aligns with the role of gut microbiota in breaking down dietary compounds into absorbable metabolites, thereby enhancing host nutrient utilization.

3.5. Probiotics induce tissue-specific transcriptional responses

To investigate the effects of probiotics on disease resistance and growth promotion in tongue sole, we analyzed the expression of related genes in the skin, liver, intestine, gills, and kidneys using transcriptomics. Compared with traditional aquaculture models, we observed that genes associated with immunity and growth were specifically expressed in the probiotic-treated group.

Specifically, a total of 3009 genes (821 up-regulated and 2188 down-regulated) exhibited differential expression in the skin; 902 genes (369 up-regulated and 533 down-regulated) in the liver; 1052 genes (262 up-regulated and 790 down-regulated) in the intestine; 1475 genes (769 up-regulated and 706 down-regulated) in the gills; and 665 genes (199 up-regulated and 466 down-regulated) in the kidneys (Fig. 5A, Detailed information on the DEGs can be found in Supplementary Materials). Our analysis revealed that some differentially expressed genes are involved

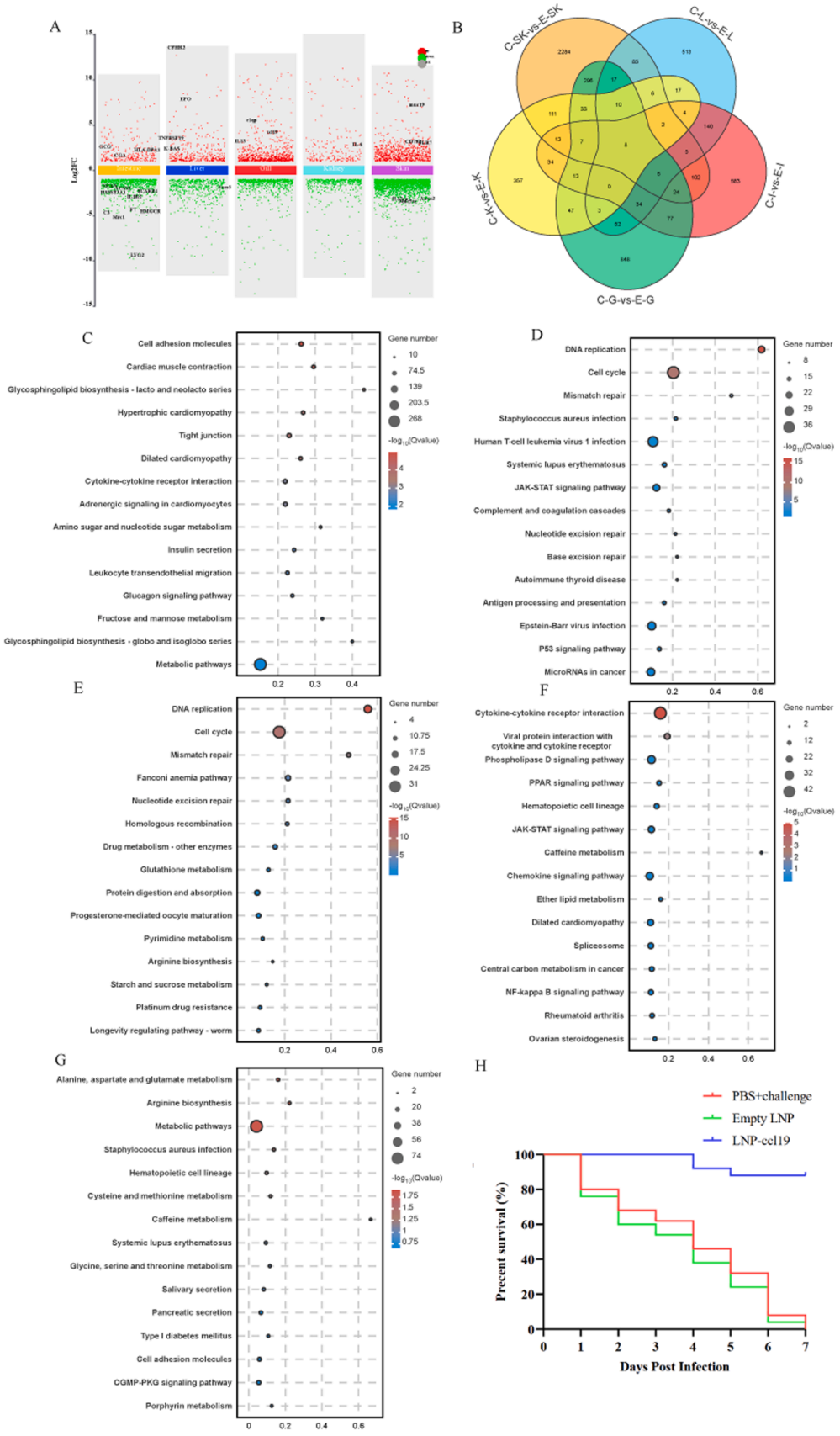

Fig. 5. Multi-tissue transcriptomic analysis of *C. semilaevis*. (A) Number of differentially expressed genes (DEGs) in each tissue (SK: skin; L: liver; I: intestine; G: gill; K: kidney). (B) Venn diagram showing shared DEGs across tissues. (C–G) Top 15 KEGG-enriched pathways in skin, intestine, liver, gill, and kidney, respectively. (H) Kaplan–Meier survival curves following *V. harveyi* challenge in fish injected with PBS, empty LNP, or LNP-*ccl19*. Each group included three replicates ($n = 50$ fish per replicate). Statistical differences were evaluated using the log-rank test ($p < 0.05$).

in immune-related processes across various tissues. Specifically: in skin tissue, immune-related genes included *OXP4, CD79B, TLR13, TLR7, IL17RD*, and *IL17C*; in intestinal tissue, immune-associated genes such as *IGHV3–30–3, HLA-DPA1, CD28*, and *TNFAI* were identified; in liver tissue, immune-related differentially expressed genes comprised complement factor H-like isoform X2, *K-BAS*, and *TNFRSF19*; in gill tissue, genes including *ccll9*, complement C1q-like protein 4, tumor necrosis factor receptor superfamily member 6B-like, and interleukin-13 receptor subunit alpha-2 were observed; in kidney tissue, *IL-6* was identified as an immune-related differentially expressed gene. Additionally, within the intestinal tissue, several differentially expressed genes were associated with growth processes, such as *igf2bp3, pyy*, and *gcg*. Venn diagram analysis revealed an overlap of 8 differentially expressed genes across all tissues (Fig. 5B), including genes related to lipid metabolism such as *acot2, RNF145, fmo5* and *tef*.

Following probiotic treatment, KEGG pathway enrichment analysis was performed on the differentially expressed genes (DEGs) in each tissue to assess the biological effects of probiotics on tongue sole. The results showed that DEGs in the skin were significantly enriched in 68 pathways ($p < 0.05$), including immune-related pathways such as leukocyte transendothelial migration and the IL-17 signaling pathway (Fig. 5C). Similarly, DEGs in the intestine were significantly enriched in 54 pathways ($p < 0.05$), with notable activation of the intestinal immune network for IgA production and antigen processing and presentation (Fig. 5D).

Additionally, DEGs in the liver, gills, and kidneys were significantly enriched in 23, 18, and 35 pathways, respectively. In the liver, DEGs were primarily associated with DNA damage repair pathways, such as mismatch repair, Fanconi anemia pathway, nucleotide excision repair, and homologous recombination (Fig. 5E). In contrast, DEGs in the gills and kidneys were predominantly enriched in immune-related pathways, including cytokine-cytokine receptor interaction, viral protein interaction with cytokine and cytokine receptor, and complement and coagulation cascades (Fig. 5F-5G).

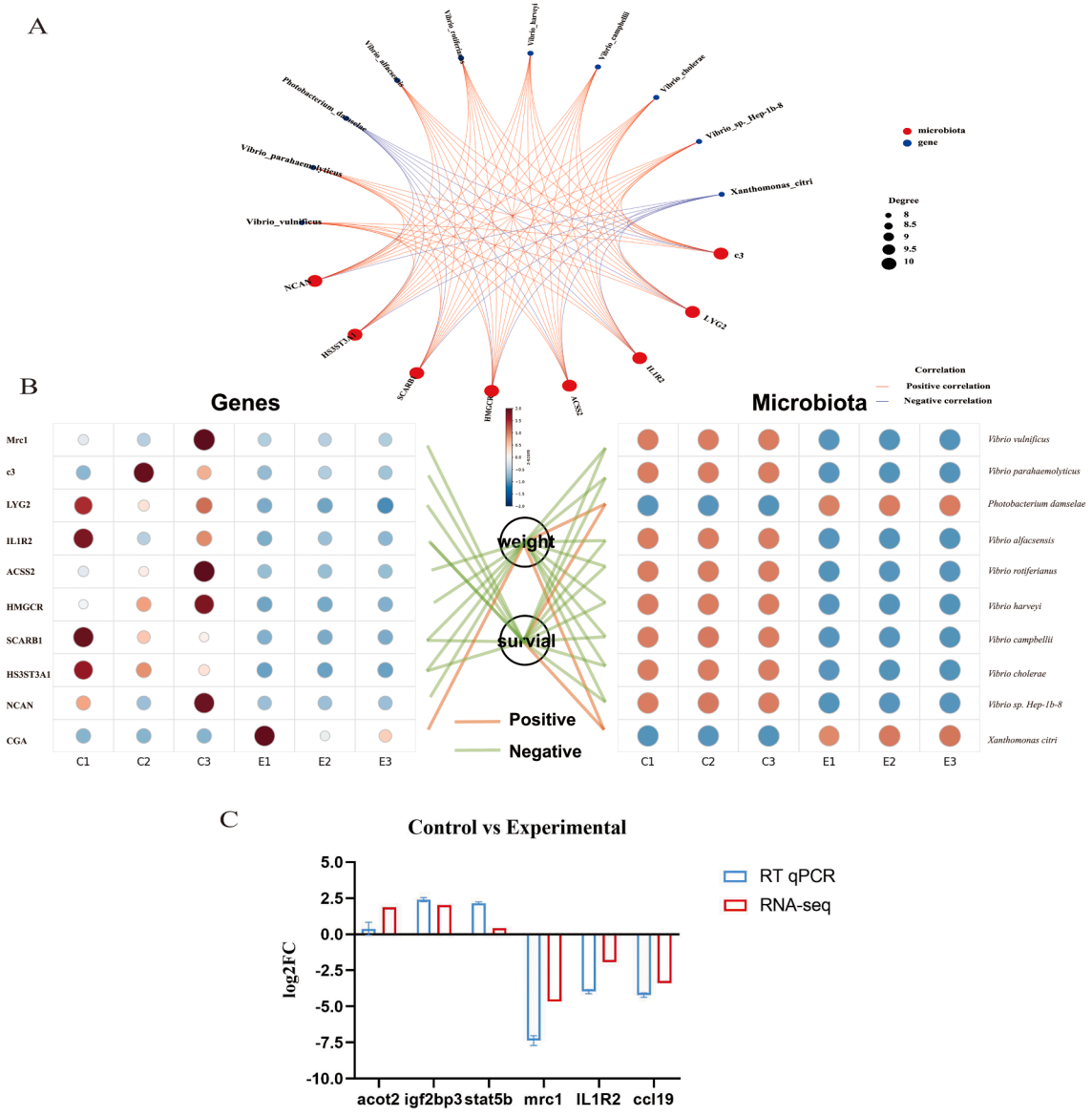

Fig. 6. Integrated analysis of host genes, microbiota, and phenotypic traits. (A) Correlation network between selected host genes and gut microbial taxa. Blue nodes represent genes, and red nodes represent microbial taxa. Edges represent significant correlations. (B) Heatmap showing associations among gene expression, microbial abundance, body weight, and survival rate. Red indicates positive correlations, and green indicates negative correlations. Correlations were calculated using Pearson correlation analysis, with significance set at $p < 0.05$. (C) Comparison of RT-qPCR and RNA-seq results for gene expression analysis.

3.6. The candidate gene provides protection against the challenge of *V. harveyi*

Based on the above transcriptome analysis results, we selected *ccl19*, which has a specifically upregulated expression level and a relatively short CDS sequence among numerous immune genes, as a candidate gene to verify whether it can resist the infection of *V.harveyi*. During the 7 days post infection, there were significant differences in the survival rates among the groups of *C.semilaevis* (Fig. 5H). In the PBS+challenge group (red curve) and the Empty LNP group (blue curve), survival declined rapidly, with mortalities beginning on day 2 post infection and reaching nearly 0 % by day 6, indicating severe infection-induced mortality. In contrast, the LNP-*ccl19* group (cyan curve) exhibited a marked protective effect, maintaining a survival rate of approximately 80–90 % at 7 days post infection, with only a few deaths observed, which was significantly higher than that of the other groups. Survival analysis showed that the LNP-*ccl19* group had a significantly higher survival probability than both the PBS and empty LNP groups (Kaplan–Meier analysis, log-rank test, $p < 0.05$).

3.7. Significant associations between key genes, microbiota, and host phenotypes

Correlation analysis between gut microbiota and differentially expressed genes identified 10 key genes, which were functionally classified based on KEGG pathways into immune-related genes (*Mrc1, c3, LYG2, IL1R2, HMGC, SCARB1, NCAN*) and growth/metabolism-related gene (*ACSS2, CGA*). According to the relationship analysis results, *P. damselae* and *X. citri* showed negative correlations with these genes, while the remaining eight Vibrio microorganisms exhibited positive correlations with these genes (Fig. 6A). Heatmap visualization further demonstrated that *Vibrio spp*. was negatively correlated with host survival rate and body weight (Fig. 6B). Most genes, particularly immune-related ones, exhibited negative correlations with both body weight and survival rate, whereas only *CGA* showed a positive correlation with body weight.

3.8. Validation of RNA-seq results by RT-qPCR for selected genes related to growth and immunity

To validate the credibility of the RNA-seq data, six genes were selected from the differential expression analysis of the intestine. Among these, three genes were related to growth (*acot2, igfbp3*, and *stat5b*), and three genes were related to immunity (*mrc1, IL1r2*, and *ccl19*). The expression of these genes was verified using the RT-qPCR method, as shown in Fig. 6C.

The results indicated that the expression trends of these selected genes were consistent with those obtained from RNA-seq. Specifically, genes related to growth (*acot2, igfbp3*, and *stat5b*) were upregulated in the experimental group compared to the control group, while immune-related genes (*mrc1, il1r2*, and *ccl19*) showed a downregulation in the experimental group. This downregulation of immune genes can be explained by the fact that in the probiotic-based aquaculture model, the host experiences less immune stress and pathogen exposure. As a result, less energy is allocated to immune responses, allowing more energy to be directed towards growth processes.

4. Discussion

This study integrates metagenomic, transcriptomic, and histological analyses to examine how a probiotic-based aquaculture strategy is associated with microbiome restructuring and host physiological responses in *C. semilaevis*, under industrial farming conditions. Unlike most previous studies conducted under laboratory conditions, this work evaluates a probiotic-based management strategy in an industrial aquaculture setting. Unlike most previous studies conducted under laboratory conditions, this work evaluates a probiotic-based management strategy in an industrial aquaculture setting.

Metagenomic analysis revealed a marked shift in gut microbial composition under the probiotic-enriched aquaculture model, with *Vibrio* dominating in the control group and Photobacterium damselae becoming the predominant taxon in the experimental group (~86 %). *Vibrio spp*., including *V. vulnificus, V. parahaemolyticus*, and *V. harveyi*, are well-recognized pathogens in tongue sole and other marine fish, often associated with disease outbreaks and substantial aquaculture losses (Han et al., 2025; Li et al., 2019; Zuo et al., 2023; Manivel et al., 2020; Ruwandeepika et al., 2012; Sony et al., 2021; Triga et al., 2023). *P. damselae* has also been reported as a pathogenic species affecting a wide range of marine fish (García-Rosado et al., 2007; Kim et al., 2009; Sharma et al., 2017; Acosta et al., 2004; Figueras et al., 1997; Labella et al., 2006; Pedersen et al., 2009; Shao et al., 2019; Wang et al., 2013), and specifically in tongue sole, *P. damselae* subsp. *damselae* has been reported to be highly pathogenic (Shao et al., 2019; Zhang et al., 2011). Although *P. damselae* was identified as *P. damselae* subsp. *piscicida* in this study (It can be identified in the intestines of both the experimental group and the control group.), which is a known pathogen in other fish species, there is currently no literature reporting pathogenic effects on tongue sole. However, the absence of such reports does not imply the absence of pathogenicity. Instead, it warrants further caution, as the enrichment of *P. damselae* subsp. *piscicida* in the gut microbiota of probiotic-treated fish requires deeper investigation. This bacterium is generally considered an opportunistic pathogen, with pathogenicity depending on host condition, environmental stress, or co-infection. While the survival rate of the experimental group remained within the normal range, the shift to *P. damselae* as the dominant species highlights the need for careful interpretation. Probiotic application may have altered the ecological structure of the gut microbiota, reducing *Vibrio* dominance potentially through competitive exclusion or quorum sensing interference, which could mitigate overall virulence pressure. In this context, *P. damselae* might occupy an ecological niche without exerting strong pathogenic effects under healthy host conditions. This interpretation is supported by studies showing that probiotics can reduce pathogen virulence through quorum sensing interference, thereby enhancing host defense mechanisms (Kiymaci et al., 2018). Nevertheless, it is important to note that this study did not assess strain-level virulence or directly evaluate the pathogenic potential of *P. damselae* subsp. *piscicida*, and its ecological and functional role in this system requires further investigation. Additionally, analysis of CAZy functions showed higher activity of CEs and AAs in the experimental group, suggesting improved carbohydrate degradation and nutrient availability, which could contribute to better host energy metabolism and potentially suppress pathogen growth indirectly (Klaysubun et al., 2024).

Histological analysis revealed improved intestinal morphology in the probiotic-treated group, including increased microvilli width and muscular layer thickness. These structural changes are likely to enhance nutrient absorption and strengthen barrier function. Such effects may be mediated by microbial metabolites, particularly short-chain fatty acids (e.g., butyrate), which are known to promote epithelial cell proliferation and intestinal integrity in vertebrates, including fish (Tran et al., 2020; Zhao et al., 2023). Similar probiotic-associated improvements in intestinal structure and function have been reported in multiple aquaculture species (Liu et al., 2026; Jahan et al., 2021).

Transcriptomic analysis indicated that probiotic treatment modulated host immune responses and growth-related processes. In particular, activation of the TLR–NF-κB signaling pathway was observed (Fig. 7), which is consistent with the well-established role of probiotic-derived microbial-associated molecular patterns (MAMPs) in stimulating host immunity (Liaqat et al., 2026; Riedel et al., 2006; Sun et al., 2014). This was accompanied by upregulation of innate immune effectors, including antimicrobial peptides and cytokine-related genes, reflecting a typical immune priming response reported in fish

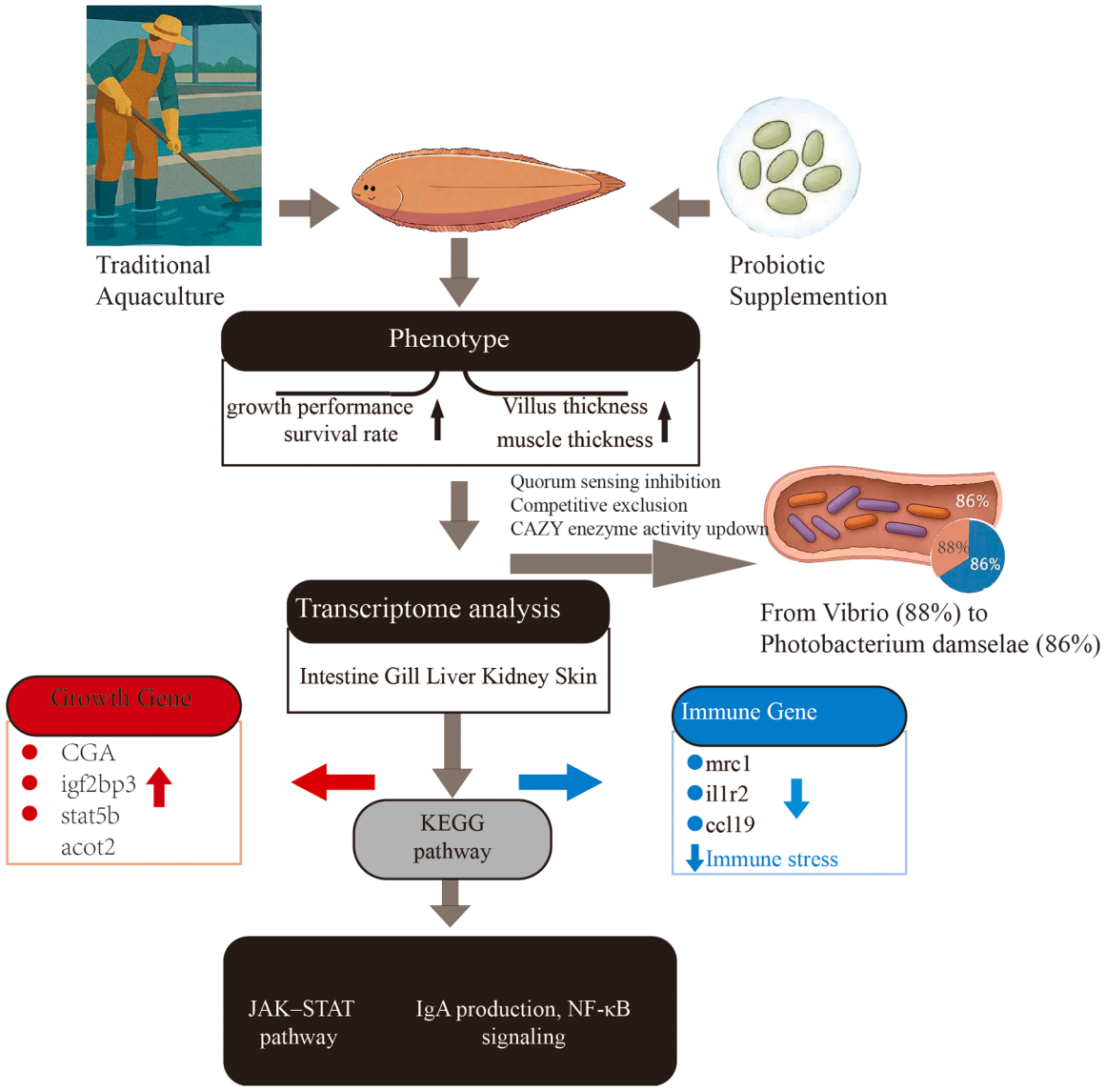

Fig. 7. Schematic overview of probiotic-associated microbiome remodeling and host responses. Conceptual model illustrating how probiotic application is associated with gut microbiome restructuring, modulation of immune pathways, and metabolic regulation, ultimately contributing to improved growth performance and disease resistance in *C.semilaevis.* This schematic is based on integrated results from metagenomic, transcriptomic, and histological analyses.

(Kitiyodom et al., 2021; Xu et al., 2017). However, the downregulation of immune-related genes in the experimental group can be explained by the reduced immune stress and pathogen exposure in this group. Under the probiotic-based aquaculture model, the host experienced less immune stress, which resulted in a decreased need for energy expenditure on immune responses. As a result, the expression of immune-related genes was downregulated, allowing for more energy to be allocated towards growth processes. Notably, *ccl19* showed differential expression in different tissues. Based on its relatively short coding sequence and its suitability for LNP-mediated delivery, this gene was selected for functional validation. The subsequent challenge experiment demonstrated that *ccl19* significantly enhanced resistance to *V. harveyi* infection, supporting its protective role in *C. semilaevis* and aligning with previous findings on CCL family genes in flatfish (Li et al., 2011, 2022; Wang et al., 2015). We fully acknowledge that the functional validation using ccl19 mRNA-LNP does not directly prove that *ccl19* is the driving factor behind the improved survival rate in the probiotic-treated group. The aim of this experiment was not to establish a direct "probiotic - *ccl19* - resistance" causal chain, but rather to serve as an alternative form of functional validation for the candidate immune genes identified through RNA-seq. While traditional qPCR validation confirms differential expression at the mRNA level, it does not address whether these genes are functionally active in disease resistance. The *ccl19* mRNA-LNP experiment demonstrated that overexpression of *ccl19* could enhance resistance to *V. harveyi*, providing indirect functional evidence for the biological relevance of the immune pathways revealed by transcriptomics. This suggests that the immune-related pathways, such as the activation of *ccl19*, may play a role in modulating disease resistance, though further studies are needed to confirm this in the context of probiotic treatment.

In terms of growth, probiotic-associated microbial metabolites, including vitamins and essential amino acids, may activate growth-related signaling pathways such as JAK–STAT, promoting protein synthesis, cell proliferation, and lipid metabolism. Consistent with this, key pathways involved in cell cycle regulation, DNA replication, and p53 signaling were also enriched, supporting enhanced somatic growth. Such nutrient- and microbiota-driven activation of growth-regulatory pathways has been widely reported as a conserved mechanism across vertebrates (Nie et al., 2021; Philip et al., 2015). These findings further support the concept of a microbiota-mediated "immune–metabolic axis,"

in which reduced immune burden allows energy reallocation toward growth and development, a process increasingly recognized in teleost host–microbe interactions (Yan et al., 2025; Zhu et al., 2022).

Correlation analysis revealed significant negative associations between the abundance of *Vibrio spp*. and several immune-related genes, including *mrc1, c3*, and *lyg2*. In the control group, where *Vibrio* dominated the gut microbiome, elevated expression of these genes suggests increased immune activation, likely reflecting higher pathogen pressure. In contrast, probiotic treatment reduced *Vibrio* abundance and was associated with decreased expression of immune-related genes, indicating a lower immune burden. This shift was accompanied by increased expression of genes related to nutrient absorption and metabolism, suggesting a reallocation of energy from immune defense toward growth processes. Together, these results support the idea that probiotics improve host performance by reducing pathogen load and optimizing energy utilization.

Overall, these findings suggest that probiotic-induced microbiome restructuring is associated with coordinated changes in host immunity, metabolism, and growth. However, as these conclusions are primarily based on correlation analyses, further functional validation is required to establish causal relationships. While the observed shift in gut microbiota towards a *P. damselae* subsp. *piscicida* -dominant community (~86 %) in the probiotic-treated group indicates significant microbial restructuring, it is important to note that *P. damselae* subsp. *piscicida* is a recognized opportunistic pathogen in marine aquaculture. Therefore, the potential risks associated with its enrichment in the gut microbiota must be carefully considered. The probiotic-integrated water management strategy demonstrated operational advantages under commercial farming conditions, including a substantial reduction in labor demand and operational cost. In a production system consisting of 48 tanks (~35 m^2 per tank), traditional management required two workers for daily manual cleaning (~15 min per tank), corresponding to approximately 6 h of labor per worker. In contrast, under the new protocol, manual cleaning was eliminated, and a single worker was able to complete water exchange and probiotic application within approximately 2 h. This represents a significant reduction in labor and operational costs, highlighting the practical feasibility and scalability of this approach. However, it should be emphasized that further studies are needed to evaluate the long-term ecological impact, safety, and potential pathogenicity of the enriched *P. damselae* subsp. *piscicida* population before recommending this strategy as a routine management practice in aquaculture systems.

Conclusion

In conclusion, our study demonstrates that the probiotic-integrated water exchange protocol provides a promising and practically relevant alternative to labor-intensive flatfish aquaculture. Probiotic treatment was associated with a marked restructuring of the gut microbiota, with a shift in dominant taxa from Vibrio-associated members to *P. damselae* subsp. *piscicida*. Multi-tissue transcriptomic analyses further revealed coordinated activation of immune pathways (e.g., NF-κB signaling and the intestinal IgA network) and growth-related signaling, including JAK–STAT-mediated metabolic regulation, supporting coordinated immune- and metabolism-related host responses in which reduced chronic immune pressure allows energy reallocation toward somatic growth. However, given the known pathogenic relevance of *P. damselae* subsp. *piscicida* in marine fish, its enrichment should not be interpreted as evidence of benefit or biosafety. The ecological role, host specificity, and pathogenic potential of this strain in the studied fish require further strain-level and functional validation.

Funding

This work was supported by National Key Research and Development Program of China (2022YFF1000303); the National Natural Science Foundation of China (32,230,107); the Key Research and Development Project of Shandong Province (2023ZLYS02, 2024CXPT071–1 and 2022ZLGX01), Central Public-interest Scientific Institution Basal Research Fund, CAFS (2023TD20, 2022CG01), Shandong Taishan Scholar Climbing Project, and Shandong Provincial Natural Science Foundation (ZR2022MC136).

Declaration of competing interest

The authors declare no competing interests.

Acknowledgements

We are sincerely grateful to the companies that provided us with aquaculture facilities and research opportunities, which were essential for this study.

Supplementary materials

Supplementary material associated with this article can be found, in the online version, at doi:10.1016/j.crmicr.2026.100600.

Data availability

The datasets presented in this study can be found in online repositories. The names of the repository/repositories and accession number(s) can be found below: NCBI [accession: PRJNA1357384].

References

Acosta, F., de Galarreta, C., Ellis, A.E., Díaz, R., Gómez, V., Padilla, D., et al., 2004. Activation of the nitric oxide response in gilthead seabream after experimental infection with Photobacterium damselae subsp piscicida. Fish. Shellfish Immunol. 16, 581–588. https://10.1016/j.fsi.2003.09.010.

Bastian, M., Heymann, S., Jacomy, M., 2009. Gephi: an open source software for exploring and manipulating networks. In: International AAAI conference on weblogs and social media. Association for the Advancement of Artificial Intelligence. CA, USA. https://10.1609/icwsm.v3i1.13937.

Benjamini, Y., Hochberg, Y., 1995. Controlling the false discovery rate: a practical and powerful approach to multiple testing. J. R. Stat. Soc. 57, 289–300. https://10.1111/j.2517-6161.1995.tb02031.x.

Bereded, N.K., Abebe, G.B., Fanta, S.W., Curto, M., Waidbacher, H., Fanta, S.W., et al., 2022. The gut bacterial microbiome of Nile tilapia (*Oreochromis niloticus*) from lakes across an altitudinal gradient. BMC. Microbiol. 22, 87. https://10.1186/s12866-022-02496-z.

Bushnell, B., 2014. BBMap: a fast, accurate, splice-aware aligner. https://www.osti.gov/biblio/1241166.

Ding, X., Jin, F., Xu, J.W., Zhang, S.L., Chen, D.X., Hu, B.J., et al., 2022. The impact of aquaculture system on the microbiome and gut metabolome of juvenile Chinese softshell turtle (*Pelodiscus sinensis*). Imeta 1, e17. https://10.1002/imt2.17.

García-Rosado, E., Cano, I., Martín-Antonio, B., Labella, A., Manchado, M., Alonso, M.C., et al., 2007. Co-occurrence of viral and bacterial pathogens in disease outbreaks affecting newly cultured sparid fish. Int. Microbiol. 10, 193–199. https://10.2436/20.1501.01.27.

Guo, Z.S., Hou, X.G., Chang, L.R., Du, Z.J., Shi, K.T., Song, A.H., et al., 2024. Effects of different feeding patterns on growth, enzyme activity, and intestinal microbiome of the juvenile Pacific abalone *Haliotis discus hannai*. Aquaculture Reporets 39, 102427. https://10.1016/j.aqrep.2024.102427.

Chen, S.F., Zhou, Y.Q., Chen, Y.R., Gu, J., 2018. fastp: an ultra-fast all-in-one FASTQ preprocessor. Bioinformatics. 34, 884–890. https://10.1093/bioinformatics/bty560.

Cui, Z.K., Liu, Y., Wang, W.W., Wang, Q., Zhang, N., Lin, F., et al., 2017. Genome editing reveals dmrt1 as an essential male sex-determining gene in Chinese tongue sole (*Cynoglossus semilaevis*). Sci. Rep. 7, 42213. https://10.1038/srep42213.

El-Gebali, S., Mistry, J., Bateman, A., Eddy, S.R., Luciani, A., Potter, S.C., et al., 2019. The Pfam protein families database in 2019. Nucleic Acids Res. 47, D427–D432. https://10.1093/nar/gky995.

Eren, A.M., Esen, O.C., Quince, C., Vineis, J.H., Morrison, H.G., Sogin, M.L., et al., 2015. Anvi'o: an advanced analysis and visualization platform for omics data. PeerJ. 3, e1319. https://10.7717/peerj.1319.

FAO, 2025. Review of the state of world marine fishery resources. Food Agric. Organiz. United Nations. https://10.4060/cd5538en.

Figueras, A., Santarem, M.M., Novoa, B., 1997. In vitro immunostimulation of turbot (Scophthalmus maximus) leucocytes with beta glucan and/or photobacterium damsela bacterin. Fish. Pathol. 32, 153–157. https://10.3147/jsfp.32.153.

Grane, D.P., Ogle, D.H., Shoup, D.E., 2020. Use and misuse of a common growth metric: guidance for appropriately calculating and reporting specific growth rate. Rev. Aquac. 12, 1542–1547. https://10.1111/raq.12396.

Han, T., Liu, Y.F., Li, M.C., Zhang, Y.T., He, Z.W., Ren, Y.Q., et al., 2025. Function of lamp2 gene response to vibrio vulnificus infection and LPS stimulation in the half-smooth tongue sole (*Cynoglossus semilaevis*). Int. J. Mol. Sci. https://10.3390/ijms26051999.

Hu, Y., Li, Y., Li, Z., Chen, C., Zang, J., Li, Y., et al.. Novel insights into the selective breeding for disease resistance to vibriosis by using natural outbreak survival data in Chinese tongue sole (*Cynoglossus semilaevis*). Aquaculture. https://10.1016/j.aquaculture.2020.735670.

Hu, Y.R., Li, Y.Z., Cheng, P., Chen, S.L., 2022. Comprehensive analysis of circular RNAs to decipher the potential roles in blind-side hypermelanosis in Chinese tongue sole (*Cynoglossus semilaevis*). Front. Mar. Sci. https://10.3389/fmars.2022.868987.

Hyatt, D., Chen, G., LoCascio, P., Land, M., Larimer, F., Hauser, L., et al., 2010. Prodigal: prokaryotic gene recognition and translation initiation site identification. BMC. Bioinformatics. 11, 119. https://10.1186/1471-2105-11-119.

Jahan, N., Islam, S.M.M., Rohani, M.F., Hossain, M.T., Shahjahan 2021., M.. Probiotic yeast enhances growth performance of rohu (Labeo rohita) through upgrading hematology, and intestinal microbiota and morphology. Aquaculture 545,737243. https://10.1016/j.aquaculture.2021.737243.

Kanehisa, M., Sato, Y., Morishima, K., 2016. BlastKOALA and GhostKOALA: KEGG tools for functional characterization of genome and metagenome sequences. J. Mol. Biol. 428, 726–731. https://10.1016/j.jmb.2015.11.006.

Kim, H.R., Kim, J.W., Lee, M.K., Kim, J.G., 2009. Septicemia progressing to fatal hepatic dysfunction in an cirrhotic patient after oral ingestion of Photobacterium damsela: a case report. Infection 37, 555–556. https://10.1007/s15010-009-9049-8.

Klaysubun, C., Chaichana, N., Suwannasin, S., Singkhamanan, K., Yaikhan, T., Kantachote, D., et al., 2024. Genomic characterization of probiotic purple nonsulfur bacteria cereibacter sphaeroides strains S3W10 and SS15: implications for enhanced shrimp aquaculture. Life-Basel 14, 1691. https://10.3390/life14121691.

Kitiyodom, S., Yata, T., Thompson, K.D., Costa, J., Elumalai, P., Katagiri, T., et al., 2021. Immersion vaccination by a biomimetic-mucoadhesive nanovaccine induces humoral immune response of red tilapia (Oreochromis sp.) against Flavobacterium columnare challenge. Vaccines (Basel) 9, 1253. https://10.3390/vaccines9111253.

Kiymaci, M.E., Altanlar, N., Gumustas, M., Ozkan, S.A., Akin, A., 2018. Quorum sensing signals and related virulence inhibition of Pseudomonas aeruginosa by a potential probiotic strain's organic acid. Microb. Pathog. 121, 190–197. https://10.1016/j.micpath.2018.05.042.

Labella, A., Vida, M., Alonso, M.C., Infante, C., Cardenas, S., Lopez-Romalde, S., et al., 2006. First isolation of photobacterium damselae ssp damselae from cultured redbanded seabream, Pagrus auriga Valenciennes, in Spain. J. Fish. Dis. 29, 175–179. https://10.1111/j.1365-2761.2006.00697.x.

Lee, M.D., 2019. GToTree: a user-friendly workflow for phylogenomics. Bioinformatics 35, 4162–4164. https://10.1093/bioinformatics/btz188.

Lee, Y., Nguyen, T.L., Roh, H., Kim, A., Park, J., Lee, J.Y., et al., 2023. Mechanisms underlying probiotic effects on neurotransmission and stress resilience in fish via transcriptomic profiling. Fish Shellfish Immunol 141, 109063. https://10.1016/j.fsi.2023.109063.

Lee, S.J., Lee, Y.S., Kim, Y.R., Jeon, M.H., Noh, D., Jeong, S.M., et al., 2025. Development of novel host-associated low-temperature probiotics (HALP) tailored to aquaculture applications. Probiotics. Antimicrob. Proteins. https://10.1007/s12602-025-10828-4.

Li, D., Liu, C.M., Luo, R., Sadakane, K., Lam, T.W., 2015. MEGAHIT: an ultra-fast single-node solution for large and complex metagenomics assembly via succinct de Bruijn graph. Bioinformatics. 31, 1674–1676. https://10.1093/bioinformatics/btv033.

Li, H., 2016. Minimap and miniasm: fast mapping and de novo assembly for noisy long sequences. Bioinformatics. 32, 2103–2110. https://10.1093/bioinformatics/btw152.

Li, H.L., Xing, J., Tang, X.Q., Sheng, X.Z., Chi, H., Zhan, W.B., et al., 2022. Two bicistronic DNA vaccines against *Vibrio anguillarum* and the immune effects on flounder Paralichthys olivaceus. J. Oceanol. Limnol. 40, 786–804. https://10.1007/s00343-021-1092-z.

Li, Y.X., Sun, J.S., Sun, L., 2011. An inflammatory CC chemokine of Cynoglossus semilaevis is involved in immune defense against bacterial infection. Fish. Shellfish. Immunol. 31, 446–452. https://10.1016/j.fsi.2011.06.017.

Li, Y.Z., Wang, L., Yang, Y.M., Li, X., Dai, H., Chen, SL., 2019a. Genetic analysis of disease resistance to *Vibrio harveyi* by challenge test in Chinese tongue sole (*Cynoglossus semilaevis*). Aquaculture 503, 430–435. https://10.1016/j.aquaculture.2019.01.011.

Liaqat, N., Li, X.N, Yang, H.C., Khan, N., Hassona, N.N., You, S.M., et al., 2026. Ammonia-hypoxia co-stress induces intestinal injury, antioxidant dysregulation, and microbial dysbiosis in *Macrobrachium rosenbergii*. Aquaculture 618, 743794. https://10.1016/j.aquaculture.2026.743794.

Liu, X., Ying, C.P., Ma, F.J., Yang, Y.P., Liu, K., 2026. Gut microbiome signatures across migratory, sedentary, and aquaculture ecotypes of *coilia nasus*. Animals 16, 840. https://10.3390/ani16050840.

Love, M.I., Huber, W., Anders, S., 2014. Moderated estimation of fold change and dispersion for RNA-seq data with DESeq2. Genome Biol. 15, 550. https://10.1186/s13059-014-0550-8.

Manivel, A., Felix, L., Nooruddin, T., Arivalagan, P., Chari, N., 2020. In vitro and in vivo biofilm forming Vibrio spp: a significant threat in aquaculture. Process Biochem. 94, 213–223. In: https://10.1016/j.procbio.2020.04.029.

Ma, Q., Zhuang, Z.M., Feng, M.R., Liu, S.F., Tang, Q.S., 2015. Evaluation of reference genes for quantitative real-time PCR analysis of gene expression during early development processes of the tongue sole (*Cynoglossus semilaevis*). ACTA Oceanologica Sinica 34, 90–97. https://10.1007/s13131-015-0725-5.

Mikheenko, A., Saveliev, V., Gurevich, A., 2016. MetaQUAST: evaluation of metagenome assemblies. Bioinformatics 32, 1088–1090. https://10.1093/bioinformatics/btv697.

Mohammed E.A.H., Ahmed, A.E.M., Kovacs, Bela., Pal, Karoly., 2025. The significance of probiotics in aquaculture: a review of research trend and latest scientific findings. Antibiotics- basel https://doi.org/10.3390/antibiotics14030242.

Nathanailides, C., Kolygas, M., Choremi, K., Mavraganis, T., Gouva, E., Vidalis, K., et al., 2021. Probiotics have the potential to significantly mitigate the environmental impact of freshwater fish farms. Fishes 6, 76. https://10.3390/fishes6040076.

Naya-Català, F., Piazzon, M.C, Torrecillas, S., Toxqui-Rodríguez, S., Calduch-Giner, J.A., Fontanillas, R., et al., 2022. Genetics and nutrition drive the gut microbiota succession and host-transcriptome interactions through the Gilthead Sea bream (*Sparus aurata*) production cycle. Biology-Basel 11, 1744. https://10.3390/biology11121744.

Nayak, S.K., 2020. Multifaceted applications of probiotic Bacillus species in aquaculture with special reference to Bacillus subtilis. Rev. Aquac. 13, 862–906. https://10.1111/raq.12503.

Nie, H.T., Zheng, M.G., Wang, Z.X., Xu, Q.Y., Yin, Z.H., Zhang, Y.M., et al., 2021. Transcriptomic analysis provides insights into candidate genes and molecular pathways involved in growth of Manila clam Ruditapes philippinarum. Funct. Integr. Genomics 21, 341–353. https://10.1007/s10142-021-00780-1.

Pedersen, K., Skall, H.F., Lassen-Nielsen, A.M., Bjerrum, L., Olesen, N.J., 2009. Photobacterium damselae subsp damselae, an emerging pathogen in Danish rainbow trout, oncorhynchus mykiss (Walbaum), mariculture. J. Fish. Dis. 32, 465–472. https://10.1016/j.fsi.2003.09.010.

Philip, A.M., Vijayan, M.M., 2015. Stress-immune-growth interactions: cortisol modulates suppressors of cytokine signaling and JAK/STAT pathway in rainbow trout liver. PLoS One 10, e0129299,. https://10.1371/journal.pone.0129299.

Qu, Z.Q., Zhou, J.Y, Li, R.J., Min, Q.W., Yi, X., Zhuang, Z.J., et al., 2025. Integrated transcriptomic and microbiota analyses reveal growth-related intestinal responses to feeding strategies in Nibea coibor. Adv. Biotechnol. 3, 37. https://10.1007/s44307-025-00088-2.

Rasmussen, J.A., Villumsen, K.R., Duchêne, D.A., Puetz, L.C., Delmont, T.O., Sveier, H., et al., 2021. Genome-resolved metagenomics suggests a mutualistic relationship between Mycoplasma and salmonid hosts. Commun. Biol. 4, 579. https://10.1038/s42003-021-02105-1.

Riedel, C.U., Foata, F., Philippe, D., Adolfsson, O., Eikmanns, B.J., Blum, S., 2006. Anti-inflammatory effects of bifidobacteria by inhibition of LPS-induced NF-κb activation. World J. Gastroenterol. 12, 3729–3735. https://10.3748/wjg.v12.i23.3729.

Ruwandeepika, H.A.D., Jayaweera, T.S.P., Bhowmick, P.P., Karunasagar, I., Bossier, P., Defoirdt, T., et al., 2012. Pathogenesis, virulence factors and virulence regulation of vibrios belonging to the Harveyi clade. Rev. Aquac. 4, 59–74. https://10.1111/j.1753-5131.2012.01061.x.

Sari, D.W.K., Khamid, N.L., Ikhrami, M.A., Hardaningsih, I., Satriyo, T.B., Suparmin, A., 2025. A metagenomic analysis of gut microbiome and growth performance of giant gourami (Osphronemus goramy) fed with raw plant-based diet. Marine Biotechnol 27, 168. https://10.1007/s10126-025-10551-9.

Schubert, M., Lindgreen, S., Orlando, L., 2016. AdapterRemoval v2: rapid adapter trimming, identification, and read merging. BMC. Res. Notes. 9, 88. https://10.1186/s13104-016-1900-2.

Shao, P., Yong, P., Zho, W., Sun, J., Wang, Y., Tang, Q., et al., 2019. First isolation of photobacterium damselae subsp. Damselae from half-smooth tongue sole suffering from skin-ulceration disease. Aquaculture 511, 734208. https://10.1016/j.aquaculture.2019.734208.

Sharma, S.P.K., Pradeep, M.A., Sadu, N., Dube, P.N., Vijayan, K.K., 2017. First report of isolation and characterization of photobacterium damselae subsp. Damselae from cage-farmed cobia (Rachycentron canadum). J. Fish. Dis. 40, 953–958. https://10.1111/jfd.12557.

Sony, M., Sumithra, T.G., Anusree, V.N., Amala, P.V., Reshma, K.J., Alex, S., Sanil, N.K., et al., 2021. Antimicrobial resistance and virulence characteristics of *Vibrio vulnificus, Vibrio parahaemolyticus* and *Vibrio harveyi* from natural disease outbreaks of marine/estuarine fishes. Aquaculture 539, 736608. https://10.1016/j.aquaculture.2021.736608.

Standen, B.T., Peggs, D.L., Rawling, M.D., Foey, A., Davies, S.J., Santos, G.A., et al., 2016. Dietary administration of a commercial mixed-species probiotic improves growth performance and modulates the intestinal immunity of tilapia. Oreochromis niloticus. Fish Shellfish Immunol. 49, 427–435. https://10.1016/j.fsi.2015.11.037.

Sun, Y.Z., Xia, H.Q., Yang, H.L., Wang, Y.L., Zou, W.C., 2014. TLR2 signaling may play a key role in the probiotic modulation of intestinal microbiota in grouper Epinephelus coioides. Aquaculture 430, 50–56. https://10.1016/j.aquaculture.2014.03.042.

Tatusov, R.L., Galperin, M.Y., Natale, D.A., Koonin, E.V., 2000. The COG database: a tool for genome-scale analysis of protein functions and evolution. Nucleic. Acids. Res. 28, 33–36. https://10.1093/nar/28.1.33.

Thy, H.T.T., Tri, N.N., Quy, O.M., Fotedar, R., Kannika, K., Unajak, S., Areechon, N., et al., 2017. Effects of the dietary supplementation of mixed probiotic spores of Bacillus amyloliquefaciens 54A, and Bacillus pumilus 47B on growth, innate immunity and stress responses of striped catfish (*Pangasianodon hypophthalmus*). Fish. Shellfish. Immunol. 60, 391–399. https://10.1016/j.fsi.2016.11.016.

Tran, N.T., Li, Z., Wang, S., Zheng, H., Aweya, J.J., Wen, X., Li, S., et al., 2020. Progress and perspectives of short-chain fatty acids in aquaculture. Rev. Aquac. 12, 283–298. https://10.1111/raq.12317.

Triga, A., Smyrli, M., Katharios, P., 2023. Pathogenic and opportunistic Vibrio spp. Associated with Vibriosis incidences in the Greek aquaculture: the role of *Vibrio harveyi* as the principal cause of vibriosis. Microorganisms 11, 1197. https://10.3390/microorganisms11051197.

Wang, H., Li, Y., Chen, K., Xia, S.D., Wang, M.Q., Sun, G.X., 2009. The feature and rule of change of growth and feed intake of *Cynoglossus semilaevis* and water quality in industrial culture with recirculation aquaculture system (in Chinese). J. Hydroecol. 30 , 52-59. https://10.15928/j.1674-3075.2009.04.023.

Wang, M.Q., Chi, H., Li, M.F., 2015. A CCL21 chemokine of tongue sole (Cynoglossus semilaevis) promotes host resistance against bacterial infection. Fish. Shellfish. Immunol. 47, 461–469. https://10.1016/j.fsi.2015.09.036.

Wang, R.X., Feng, J., Su, Y.L., Ye, L.T., Wang, J.Y., 2013. Studies on the isolation of photobacterium damselae subsp piscicida from diseased golden pompano (Trachinotus ovatus Linnaeus) and antibacterial agents sensitivity. Vet. Microbiol. 162, 957–963. https://10.1016/j.vetmic.2012.09.020.

Wang, X., Liu, S., Sun, Y., Yu, X., Lee, S.M., Cheng, Q., Wei, T., et al., 2023. Preparation of selective organ-targeting (SORT) lipid nanoparticles (LNPs) using multiple technical methods for tissue-specific mRNA delivery. Nat. Protoc. 18, 265–291. https://10.1038/s41596-022-00755-x.

Wang, Y., Wang, QK., Xing, KZ., Jiang, P., Wang, J.R., 2021. Dietary cinnamaldehyde and Bacillus subtilis improve growth performance, digestive enzyme activity, and antioxidant capability and shape intestinal microbiota in tongue sole, *Cynoglossus semilaevis*. Aquaculture 531, 735798. https://10.1016/j.aquaculture.2020.735798.

Xie, J.J., Liu, Q.Q., Liao, S., Fang, H.H., Yin, P., Xie, S.W., et al., 2019. Effects of dietary mixed probiotics on growth, non-specific immunity, intestinal morphology and microbiota of juvenile pacific white shrimp, *Litopenaeus vannamei*. Fish. Shellfish. Immunol. 90, 456–465. https://10.1016/j.fsi.2019.04.301.

Xu, D.H., Moreira, G.S.A., Shoemaker, C.A., Zhang, D.H., Beck, B.H., 2017. Expression of immune genes in systemic and mucosal immune tissues of channel catfish vaccinated with live theronts of Ichthyophthirius multifiliis. Fish. Shellfish. Immunol. 66, 540–547. https://10.1016/j.fsi.2017.05.051.

Yan, W.L., Zhang, K., Guo, J., Xu, L.F., 2025. Bile acid-mediated gut-liver axis crosstalk: the role of nuclear receptor signaling in dynamic regulation of inflammatory networks. Front. Immunol. 16, 1595486. https://10.3389/fimmu.2025.1595486.

Zhang, X.J., Qin, G.M., Bing, G.M., Yan, B.L., Bi, K.R., 2011. Phenotypic and molecular characterization of photobacterium damselae, a pathogen of the cultured tongue sole *cynoglossus semilaevis* in China. N. Z. J. Mar. Freshwater Res. 45, 1–13. https://10.1080/00288330.2010.531745.

Zhao, C.Y., Men, X., Dang, Y.J., Zhou, Y.E., Ren, Y.C., 2023. Probiotics mediate intestinal microbiome and microbiota-derived metabolites regulating the growth and immunity of Rainbow Trout (*Oncorhynchus mykiss*). Microbiol. Spectr. 11, 03980. https://10.1128/spectrum.03980-22.

Zheng, W.W., Chen, Y.D., Yang, T., Liu, Z.H., Xu, D., Han, H.Z., et al., 2025. Interactions between the intestinal microbiome and host genes in regulating vibriosis resistance in *Cynoglossus semilaevis*. Front. Immunol. 16, 1644885. https://10.3389/fimmu.2025.1644885.

Zhu, W.F., Zhou, Y., Tsao, R., Dong, H.H., Zhang, H., 2022. Amelioratory effect of resistant starch on non-alcoholic fatty liver disease via the gut-liver axis. Front. Nutr. 9, 861854. https://10.3389/fnut.2022.861854.

Zuo, Z., Shang, B., Liu, H., Sun, J., Li, W., Liu, Y., et al., 2023. Identification and evaluation of potential probiotics against skin-ulceration disease in the Chinese tongue sole (*Cynoglossus semilaevis*). Fish. Shellfish. Immunol. 137,108769. https://10.1016/j.fsi.2023.108769.